

Gamma-ray flares from the Crab Nebula

A. A. Abdo¹, M. Ackermann², M. Ajello², A. Allafort², L. Baldini³, J. Ballet⁴, G. Barbiellini^{5,6}, D. Bastieri^{7,8}, K. Bechtol², R. Bellazzini³, B. Berenji², R. D. Blandford^{2,*}, E. D. Bloom², E. Bonamente^{9,10}, A. W. Borgland², A. Bouvier², T. J. Brandt^{11,12}, J. Bregeon³, A. Brez³, M. Brigida^{13,14}, P. Bruel¹⁵, R. Buehler^{2,†}, S. Buson^{7,8}, G. A. Caliandro¹⁶, R. A. Cameron², A. Cannon^{17,18}, P. A. Caraveo¹⁹, J. M. Casandjian⁴, Ö. Çelik^{17,20,21}, E. Charles², A. Chekhtman²², C. C. Cheung¹, J. Chiang², S. Ciprini¹⁰, R. Claus², J. Cohen-Tanugi²³, L. Costamante², S. Cutini²⁴, F. D'Ammando^{25,26}, C. D. Dermer²⁷, A. de Angelis²⁸, A. de Luca²⁹, F. de Palma^{13,14}, S. W. Digel², E. do Couto e Silva², P. S. Drell², A. Drlica-Wagner², R. Dubois², D. Dumora³⁰, C. Favuzzi^{13,14}, S. J. Fegan¹⁵, E. C. Ferrara¹⁷, W. B. Focke², P. Fortin¹⁵, M. Frailis^{28,31}, Y. Fukazawa³², S. Funk^{2,‡}, P. Fusco^{13,14}, F. Gargano¹⁴, D. Gasparrini²⁴, N. Gehrels¹⁷, S. Germani^{9,10}, N. Giglietto^{13,14}, F. Giordano^{13,14}, M. Giroletti³³, T. Glanzman², G. Godfrey², I. A. Grenier⁴, M.-H. Grondin³⁰, J. E. Grove²⁷, S. Guiriec³⁴, D. Hadasch¹⁶, Y. Hanabata³², A. K. Harding¹⁷, K. Hayashi³², M. Hayashida², E. Hays¹⁷, D. Horan¹⁵, R. Itoh³², G. Jóhannesson³⁵, A. S. Johnson², T. J. Johnson^{17,36}, D. Khangulyan⁴², T. Kamae², H. Katagiri³², J. Kataoka³⁷, M. Kerr³⁸, J. Knödlseeder¹¹, M. Kuss³, J. Lande², L. Latronico³, S.-H. Lee², M. Lemoine-Goumard³⁰, F. Longo^{5,6}, F. Loparco^{13,14}, P. Lubrano^{9,10}, G. M. Madejski², A. Makeev²², M. Marelli¹⁹, M. N. Mazziotta¹⁴, J. E. McEnery^{17,36}, P. F. Michelson², W. Mitthumsiri², T. Mizuno³², A. A. Moiseev^{20,36}, C. Monte^{13,14}, M. E. Monzani², A. Morselli³⁹, I. V. Moskalenko², S. Murgia², T. Nakamori³⁷, M. Naumann-Godo⁴, P. L. Nolan², J. P. Norris⁴⁰, E. Nuss²³, T. Ohsugi⁴¹, A. Okumura⁴², N. Omodei², J. F. Ormes⁴⁰, M. Ozaki⁴², D. Paneque², D. Parent²², V. Pelassa²³, M. Pepe^{9,10}, M. Pesce-Rollins³, M. Pierbattista⁴, F. Piron²³, T. A. Porter², S. Rainò^{13,14}, R. Rando^{7,8}, P. S. Ray²⁷, M. Razzano³, A. Reimer^{43,2}, O. Reimer^{43,2}, T. Reposeur³⁰, R. W. Romani², H. F.-W. Sadrozinski⁴⁴, D. Sanchez¹⁵, P. M. Saz Parkinson⁴⁴, J. D. Scargle⁴⁵, T. L. Schalk⁴⁴, C. Sgrò³, E. J. Siskind⁴⁶, P. D. Smith¹², G. Spandre³, P. Spinelli^{13,14}, M. S. Strickman²⁷, D. J. Suson⁴⁷, H. Takahashi⁴¹, T. Takahashi⁴², T. Tanaka², J. B. Thayer², D. J. Thompson¹⁷, L. Tibaldo^{7,8,4,48}, D. F. Torres^{16,49}, G. Tosti^{9,10}, A. Tramacere^{2,50,51}, E. Troja^{17,52}, Y. Uchiyama², J. Vandenbroucke², V. Vasileiou^{20,21}, G. Vianello^{2,50}, V. Vitale^{39,53}, P. Wang², K. S. Wood²⁷, Z. Yang^{54,55}, M. Ziegler⁴⁴

1. National Research Council Research Associate, National Academy of Sciences, Washington, DC 20001, resident at Naval Research Laboratory, Washington, DC 20375, USA
2. W. W. Hansen Experimental Physics Laboratory, Kavli Institute for Particle Astrophysics

- and Cosmology, Department of Physics and SLAC National Accelerator Laboratory, Stanford University, Stanford, CA 94305, USA
3. Istituto Nazionale di Fisica Nucleare, Sezione di Pisa, I-56127 Pisa, Italy
 4. Laboratoire AIM, CEA-IRFU/CNRS/Université Paris Diderot, Service d'Astrophysique, CEA Saclay, 91191 Gif sur Yvette, France
 5. Istituto Nazionale di Fisica Nucleare, Sezione di Trieste, I-34127 Trieste, Italy
 6. Dipartimento di Fisica, Università di Trieste, I-34127 Trieste, Italy
 7. Istituto Nazionale di Fisica Nucleare, Sezione di Padova, I-35131 Padova, Italy
 8. Dipartimento di Fisica "G. Galilei", Università di Padova, I-35131 Padova, Italy
 9. Istituto Nazionale di Fisica Nucleare, Sezione di Perugia, I-06123 Perugia, Italy
 10. Dipartimento di Fisica, Università degli Studi di Perugia, I-06123 Perugia, Italy
 11. Centre d'Étude Spatiale des Rayonnements, CNRS/UPS, BP 44346, F-30128 Toulouse Cedex 4, France
 12. Department of Physics, Center for Cosmology and Astro-Particle Physics, The Ohio State University, Columbus, OH 43210, USA
 13. Dipartimento di Fisica "M. Merlin" dell'Università e del Politecnico di Bari, I-70126 Bari, Italy
 14. Istituto Nazionale di Fisica Nucleare, Sezione di Bari, 70126 Bari, Italy
 15. Laboratoire Leprince-Ringuet, École polytechnique, CNRS/IN2P3, Palaiseau, France
 16. Institut de Ciències de l'Espai (IEEC-CSIC), Campus UAB, 08193 Barcelona, Spain
 17. NASA Goddard Space Flight Center, Greenbelt, MD 20771, USA
 18. University College Dublin, Belfield, Dublin 4, Ireland
 19. INAF-Istituto di Astrofisica Spaziale e Fisica Cosmica, I-20133 Milano, Italy
 20. Center for Research and Exploration in Space Science and Technology (CRESST) and NASA Goddard Space Flight Center, Greenbelt, MD 20771, USA
 21. Department of Physics and Center for Space Sciences and Technology, University of Maryland Baltimore County, Baltimore, MD 21250, USA

22. College of Science, George Mason University, Fairfax, VA 22030, resident at Naval Research Laboratory, Washington, DC 20375, USA
23. Laboratoire de Physique Théorique et Astroparticules, Université Montpellier 2, CNRS/IN2P3, Montpellier, France
24. Agenzia Spaziale Italiana (ASI) Science Data Center, I-00044 Frascati (Roma), Italy
25. IASF Palermo, 90146 Palermo, Italy
26. INAF-Istituto di Astrofisica Spaziale e Fisica Cosmica, I-00133 Roma, Italy
27. Space Science Division, Naval Research Laboratory, Washington, DC 20375, USA
28. Dipartimento di Fisica, Università di Udine and Istituto Nazionale di Fisica Nucleare, Sezione di Trieste, Gruppo Collegato di Udine, I-33100 Udine, Italy
29. Istituto Universitario di Studi Superiori (IUSS), I-27100 Pavia, Italy
30. Université Bordeaux 1, CNRS/IN2p3, Centre d'Études Nucléaires de Bordeaux Gradignan, 33175 Gradignan, France
31. Osservatorio Astronomico di Trieste, Istituto Nazionale di Astrofisica, I-34143 Trieste, Italy
32. Department of Physical Sciences, Hiroshima University, Higashi-Hiroshima, Hiroshima 739-8526, Japan
33. INAF Istituto di Radioastronomia, 40129 Bologna, Italy
34. Center for Space Plasma and Aeronomic Research (CSPAR), University of Alabama in Huntsville, Huntsville, AL 35899, USA
35. Science Institute, University of Iceland, IS-107 Reykjavik, Iceland
36. Department of Physics and Department of Astronomy, University of Maryland, College Park, MD 20742, USA
37. Research Institute for Science and Engineering, Waseda University, 3-4-1, Okubo, Shinjuku, Tokyo, 169-8555 Japan
38. Department of Physics, University of Washington, Seattle, WA 98195-1560, USA
39. Istituto Nazionale di Fisica Nucleare, Sezione di Roma "Tor Vergata", I-00133 Roma, Italy
40. Department of Physics and Astronomy, University of Denver, Denver, CO 80208, USA

41. Hiroshima Astrophysical Science Center, Hiroshima University, Higashi-Hiroshima, Hiroshima 739-8526, Japan
42. Institute of Space and Astronautical Science, JAXA, 3-1-1 Yoshinodai, Chuo-ku, Sagami-hara, Kanagawa 252-5210, Japan
43. Institut für Astro- und Teilchenphysik and Institut für Theoretische Physik, Leopold-Franzens-Universität Innsbruck, A-6020 Innsbruck, Austria
44. Santa Cruz Institute for Particle Physics, Department of Physics and Department of Astronomy and Astrophysics, University of California at Santa Cruz, Santa Cruz, CA 95064, USA
45. Space Sciences Division, NASA Ames Research Center, Moffett Field, CA 94035-1000, USA
46. NYCB Real-Time Computing Inc., Lattingtown, NY 11560-1025, USA
47. Department of Chemistry and Physics, Purdue University Calumet, Hammond, IN 46323-2094, USA
48. Partially supported by the International Doctorate on Astroparticle Physics (IDAPP) program
49. Institució Catalana de Recerca i Estudis Avançats (ICREA), Barcelona, Spain
50. Consorzio Interuniversitario per la Fisica Spaziale (CIFS), I-10133 Torino, Italy
51. INTEGRAL Science Data Centre, CH-1290 Versoix, Switzerland
52. NASA Postdoctoral Program Fellow, USA
53. Dipartimento di Fisica, Università di Roma “Tor Vergata”, I-00133 Roma, Italy
54. Department of Physics, Stockholm University, AlbaNova, SE-106 91 Stockholm, Sweden
55. The Oskar Klein Centre for Cosmoparticle Physics, AlbaNova, SE-106 91 Stockholm, Sweden

† buehler@stanford.edu, * rdb3@stanford.edu , ‡funk@slac.stanford.edu

A young and energetic pulsar powers the well-known Crab Nebula. Because of its bright and apparently steady emission it has been used as a reference source to calibrate telescopes in several wavebands, in particular at high energies. Here we report two separate gamma-ray (photon energy >100 MeV) flares from this source detected by the Large Area Telescope on board the Fermi Gamma-ray Space Telescope. The first flare occurred in February 2009 and lasted approximately sixteen days. The second flare was detected in September 2010 and lasted approximately four days. During these two outbursts the gamma-ray flux from the nebula increased by factors of four and six, respectively. The brevity of the flares implies that the gamma rays are emitted via synchrotron radiation from PeV (10^{15} eV) electrons in a region smaller than 1.4×10^{-2} pc. These are the highest energy particles that can be associated with a discrete astronomical source, and they pose special challenges to particle acceleration theory.

The Crab Nebula is the remnant of an historical supernova (SN), recorded in 1054 AD, located at a distance of 2 kpc (1). The SN explosion left behind a pulsar, which continuously emits a wind of magnetized plasma of electron/positron pairs (henceforth referred to as electrons). This pulsar wind is expected to terminate in a standing shock where pressure balance is attained with the ambient medium (2). At this location, the electrons are thermalized and may undergo shock acceleration (3). As the electrons diffuse into the downstream medium they release energy through interactions with the surrounding magnetic and photon fields. This emission is observed across all wavebands from radio up to TeV gamma-ray energies and is referred to as a pulsar wind nebula (PWN). The efficiency of this process is remarkable. As much as 30% of the total energy released by the Crab pulsar is emitted by the PWN (4). For a review of PWNe see e.g. Gaensler & Slane 2006 (5).

The Crab PWN has an approximately ellipsoidal shape on the sky with a size that decreases with increasing photon energy. At radio frequencies it extends out to $5'$ (3 pc) from the central pulsar. At X-ray wavelengths a bright torus surrounds the pulsar; assuming axial symmetry it has a radius of $40''$ (0.4 pc) and jets are observed to emerge perpendicular to it in both directions. Within the region encapsulated by the torus there are several small-scale structures. The inner nebula, which we define as the central $15''$ around the pulsar, has several small-scale features of variable X-ray and optical brightness. The most prominent is an X-ray-bright inner ring with a radius of $10''$ (0.1 pc), which is attributed to the termination shock of the PWN (6). Several knots with diameters of $\sim 1''$ (0.01 pc) are detected close to the inner ring and the base of the jets, and bright arcs of comparable width are observed moving outwards from the inner ring into the torus (7, 8).

The broad-band spectral energy distribution (SED) of the Crab Nebula is composed of two broad non-thermal components. A low-energy component dominates the overall energy output and extends from radio to gamma-ray frequencies. The emission from this component is thought to be from synchrotron radiation. This is confirmed from radio to X-ray frequencies

with polarization measurements (9–11). The emission of this synchrotron component peaks between optical and X-ray frequencies, where the emission is primarily from the torus (6). The emission site of higher-energy photons (beyond 100 keV) cannot be resolved due to the limited angular resolution of telescopes observing at these frequencies. The high-energy component dominates the emission above ~ 400 MeV and is thought to be emitted via inverse Compton (IC) scattering, predominantly of the synchrotron photons (12, 13).

The large-scale integrated emission from the Crab Nebula is expected to be steady within a few percent and is thus often used to cross-calibrate X-ray and gamma-ray telescopes and to check their stability over time (14, 15). Recently, flux variability of the nebula of the order of $\sim 3.5\%$ yr^{-1} has been detected in the X-ray band, setting limits on the accuracy of this practice (16). Evidence for flux variations on yearly time-scales was also reported for the emission in the high-energy tail (1–150 MeV) of the synchrotron component (17, 18). No significant flux variations have been detected for the high-energy component of the nebula (19–21). For a review of the Crab Nebula see, e.g., Hester 2008 (4).

The Large Area Telescope (LAT) on board the Fermi Gamma-Ray Space Telescope (Fermi) has continuously monitored the Crab Nebula as a part of its all-sky survey since August 2008. The LAT detects gamma rays in the energy range 20 MeV to >300 GeV, and this spans the transition region between the low and the high-energy components of the nebular spectrum. The average SED measured during the first 25 months of observations is shown in Figure 1. It is well characterized by the sum of two spectral components, each with a power-law dependence on energy (22). The photon index of the low-energy component is 3.69 ± 0.11 . The high-energy component has a hard spectrum with a photon index of 1.67 ± 0.04 . The 25-month average photon flux above 100 MeV of the synchrotron and IC components are $(6.2 \pm 0.3) \times 10^{-7} \text{ cm}^{-2} \text{ s}^{-1}$ and $(1.3 \pm 0.1) \times 10^{-7} \text{ cm}^{-2} \text{ s}^{-1}$ respectively (only statistical errors are given; see online supplements for a discussion of systematic errors).

In order to search for flux variability of both spectral components in the LAT band, the flux measurement was performed in monthly time bins. While the high-energy component was found to be stable, the low-energy component is variable on these time scales. Figure 2 shows the integral flux of this component as a function of time. The probability to measure the observed flux variations in the case of a constant source due to statistical fluctuations is less than 10^{-5} . No significant spectral variations were detected for either component on monthly time scales. Flux variability was also searched for on sub-monthly time scales, for which the low-energy component of the nebula is significantly detected by the LAT only in high-flux states.

Two time periods with significantly enhanced flux compared to the average values were identified: one in February 2009, the other in September 2010. The flux of the low-energy component as a function of time is shown in Figure 2 in four-day time bins around these periods. The first flare had a duration of ~ 16 days. The average integral flux above 100 MeV of the low-energy component between MJD 54857.73 and 54873.73 was $(23.2 \pm 2.9) \times 10^{-7} \text{ cm}^{-2} \text{ s}^{-1}$, corresponding to a flux increase of a factor 3.8 ± 0.5 compared with the average value; the increase is significant at $>8\text{-}\sigma$ level. The second flare, first reported by the AGILE gamma-ray mission (23), lasted for only 4 days. The integral flux above 100 MeV between MJD 55457.73

and 55461.73 was $(33.8 \pm 4.6) \times 10^{-7} \text{ cm}^{-2} \text{ s}^{-1}$, corresponding to a flux increase of a factor 5.5 ± 0.8 with respect to the average and a significance of $>10 \sigma$. The energy spectra during both flares is shown in Figure 1. The first flare has a soft spectrum with a photon index of 4.3 ± 0.3 . The spectral slope is compatible with the average 25-month value within two standard deviations. The energy spectrum measured for the second flare is significantly harder, with a photon index of 2.7 ± 0.2 , and is still detected above 1 GeV at a $3\text{-}\sigma$ -level. The average power released in each of the gamma-ray flares is approximately $4 \times 10^{36} \text{ erg s}^{-1}$, assuming isotropic emission. We note that no significant variations in the emission of the pulsar were detected on monthly and four-day time scales through the period of observations. Examination of the timing residuals of the pulsed emission indicated no significant variations during either flares nor any significant glitch activity during the first 25 months of LAT observations. For more on this and the LAT analysis see the supporting online material.

Several observations of the synchrotron component between infrared and X-ray frequencies were performed to search for flux variability related to the gamma-ray emission during the second flare (24). They revealed no deviations from the average nebular flux level. We analyzed data collected by the BAT instrument on board the Swift satellite (25), which continuously monitors the sky at photon energies of 15–150 keV. The mean flux measured during the first flare is $(2.0 \pm 0.1) \times 10^{-8} \text{ erg cm}^{-2} \text{ s}^{-1}$, the flux during the second flare is $(2.0 \pm 0.1) \times 10^{-8} \text{ erg cm}^{-2} \text{ s}^{-1}$. Both observations are therefore within 5% of the average flux of $(2.09 \pm 0.10) \times 10^{-8} \text{ erg cm}^{-2} \text{ s}^{-1}$ measured by BAT in this energy range (26), and show no correlation to the gamma-ray flares. Note that the angular resolution of the BAT only allows for the measurement of the spatially integrated spectrum. Sub-arc-second resolution images were taken in X-rays by the Chandra observatory and optical by the Hubble Space Telescope a few days after the second flare. While both observations revealed no unusual activity compared to previous observations, it should be noted that both show a brightening $3''$ east of the pulsar (27). In the Chandra image this brightening is associated with a knot of $\sim 1''$ diameter that might be associated with the inner ring or the base of the jet. Such a brightening might be interpreted as an afterglow at lower frequencies of the gamma-ray flare, but no conclusions can be drawn based on one event.

The brief flare time scales and the requirement that the emission volume be causally connected imply that the flaring region must be compact. If L is the diameter of the flaring region along the line-of-sight and t is the flare duration, then $L < Dct$, where the Doppler factor D accounts for relativistic boosting effects. The Doppler factor is expected to be moderate within the Crab Nebula, as the typical velocities observed are smaller than $0.9 c$ (8, 28). Even assuming that the emission region is moving directly toward us, this yields $D < 4.4$. For a flare duration of 4 days this results in $L < 1.4 \times 10^{-2} \text{ pc}$, which corresponds to $<1.5''$ projected on the sky. Structures this small are found only in the inner part of the nebula, close to the termination shock or the base of the jet, suggesting that the gamma-ray emission detected in the flare originates from these regions. This is consistent with relativistic magnetohydrodynamic (MHD) simulations, which assume that the gamma-ray emission of the synchrotron component originates close to the termination shock (28–30).

The spectral shape of the low-energy component in the LAT energy range and its extrapo-

lation to the emission at lower energies suggest that it is emitted via synchrotron emission. The brevity of the gamma-ray flares strengthens this scenario: If the flare were instead produced by IC radiation or Bremsstrahlung, the cooling time of the emitting electrons would greatly exceed the flare duration. The cooling via Bremsstrahlung in particle densities $< 10 \text{ cm}^{-3}$ (31) happens on time scales of $\sim 10^6$ years. Similarly, electrons cooling via IC emission of 100 MeV gamma rays on the photons of the synchrotron component of Crab Nebula have cooling times $\gtrsim 10^7$ years. The average magnetic field inside the Crab Nebula is estimated to be $\sim 200 \text{ } \mu\text{G}$, as deduced from modeling of the broad-band SED (13, 22), and might be enhanced locally by up to an order of magnitude in the inner nebula (32). These fields imply synchrotron cooling times $\lesssim 15$ days, comparable to the flare duration, leaving synchrotron radiation as the only plausible process responsible for the gamma-ray emission during the flares.

The detection of synchrotron photons up to energies of $> 1 \text{ GeV}$ confirms that electrons are accelerated to energies of $\gtrsim 1 \text{ PeV}$ in the Crab Nebula (33). These are the highest energy particles that can be associated directly with any astronomical source, and they pose special challenges to particle acceleration theory. Because synchrotron losses are so efficient, there must be a strong electric field E to compensate radiation reaction, given by:

$$E/B \sim r_L/\ell_{\text{cool}} \lesssim (1.5\alpha\mathcal{E}_{\gamma\text{pk}}/m_e c^2) \sim (\mathcal{E}_{\gamma\text{pk}}/50\text{MeV}) \quad (1)$$

where r_L is the Larmor radius, ℓ_{cool} is the radiative cooling length, α is the fine structure constant and $\mathcal{E}_{\gamma\text{pk}}$ is the peak energy in the gamma-ray spectrum emitted by the most energetic electrons accelerated ($\mathcal{E}_{\gamma\text{pk}}$ may be a factor no more than ~ 5 lower than the maximum photon energy observed) (18, 34). The electric field is very unlikely to exceed the magnetic field; if it did, there would be a local reference frame with pure electric field in which vacuum breakdown would occur very quickly. We conclude that the electric field, as measured in the Crab frame, is close in magnitude to the magnetic field in the region where the highest energy synchrotron photons are emitted. This subsumes the possibility of bulk relativistic motion. Furthermore, the resistive force due to radiation reaction is competitive with the Lorentz force and the cooling length is comparable with the Larmor radius. This poses severe difficulties to the widely-discussed acceleration mechanism of diffusive shock acceleration (35). The proposed acceleration due to absorption of ion cyclotron waves does not suffer from these constraints. However, it appears to operate on time scales which are too long to accommodate the fast variability seen during the flares (36). Alternatively, the acceleration could be related directly to the electric field from the pulsar.

The Crab Nebula is powered by the central neutron star which acts as a DC unipolar inductor and a source of an AC “striped” wind (2, 3). Using the measured spin-down rate, a moment of inertia of $\sim 1 \times 10^{45} \text{ g cm}^2$ and a force-free model of the magnetosphere, the total induced potential difference is $\sim 50 \text{ PV}$ and the associated current is $\sim 300 \text{ TA}$ with an associated DC power per hemisphere of $\sim 1.5 \times 10^{38} \text{ erg s}^{-1}$. What happens to the DC and AC current flows is controversial. It is widely supposed that $\sim 90\%$ of the DC current returns in an outflowing wind which becomes particle-dominated and shocks at a (mostly invisible) termination shock with radius $\sim 0.1 \text{ pc}$ (37). Alternatively, the wind could remain electromagnetically dominated

with most of the dissipation and associated flux removal occurring along the polar axis at the jet and/or in the equatorial plane at the torus (34, 38). The AC component may also disappear through reconnection in the wind or survive to contribute to the nebular particle acceleration.

The variable part of the gamma-ray luminosity in the 0.1–1 GeV band is $L_\gamma \sim 10^{35}$ erg s⁻¹, or roughly 10^{-3} of the DC pulsar power and a similar fraction of the total bolometric power of the nebula, which is dominated by optical emission. If we make conservative assumptions about the spectrum - $\mathcal{E}_{\gamma\text{pk}} \sim 200$ MeV - and assume a field of B_{-3} mG, at least $\Phi_{\text{acc}} \sim 3B_{-3}^{-1/2}$ PV of potential difference must be maintained across a Larmor radius/cooling length $\sim 10^{16} B_{-3}^{-3/2}$ cm. The observed variability time scale of 10^6 s then suggests that $B_{-3} > 0.5$, larger than associated with the termination shock of a particle-dominated wind, and an accelerating potential difference satisfying $4 \text{ PV} < \Phi_{\text{acc}} < 50 \text{ PV}$. The current flowing through the acceleration site carried by the highest energy electrons is then $\sim L_\gamma/\Phi_{\text{acc}} \sim 0.3 - 3$ TA, significantly less than the current flowing through the neutron star estimated above.

The observations reported here have raised compelling questions on our understanding of particle acceleration and motivate more detailed calculations; together with the ongoing gamma-ray observations of the LAT and observational campaigns at X-ray and optical wavelengths they might soon pinpoint the gamma-ray emission site in the Crab Nebula.

The Fermi LAT Collaboration acknowledges generous ongoing support from a number of agencies and institutes that have supported both the development and the operation of the LAT as well as scientific data analysis. These include the National Aeronautics and Space Administration and the Department of Energy in the United States, the Commissariat à l’Energie Atomique and the Centre National de la Recherche Scientifique / Institut National de Physique Nucléaire et de Physique des Particules in France, the Agenzia Spaziale Italiana and the Istituto Nazionale di Fisica Nucleare in Italy, the Ministry of Education, Culture, Sports, Science and Technology (MEXT), High Energy Accelerator Research Organization (KEK) and Japan Aerospace Exploration Agency (JAXA) in Japan, and the K. A. Wallenberg Foundation, the Swedish Research Council and the Swedish National Space Board in Sweden. Additional support for science analysis during the operations phase is gratefully acknowledged from the Istituto Nazionale di Astrofisica in Italy and the Centre National d’Études Spatiales in France.

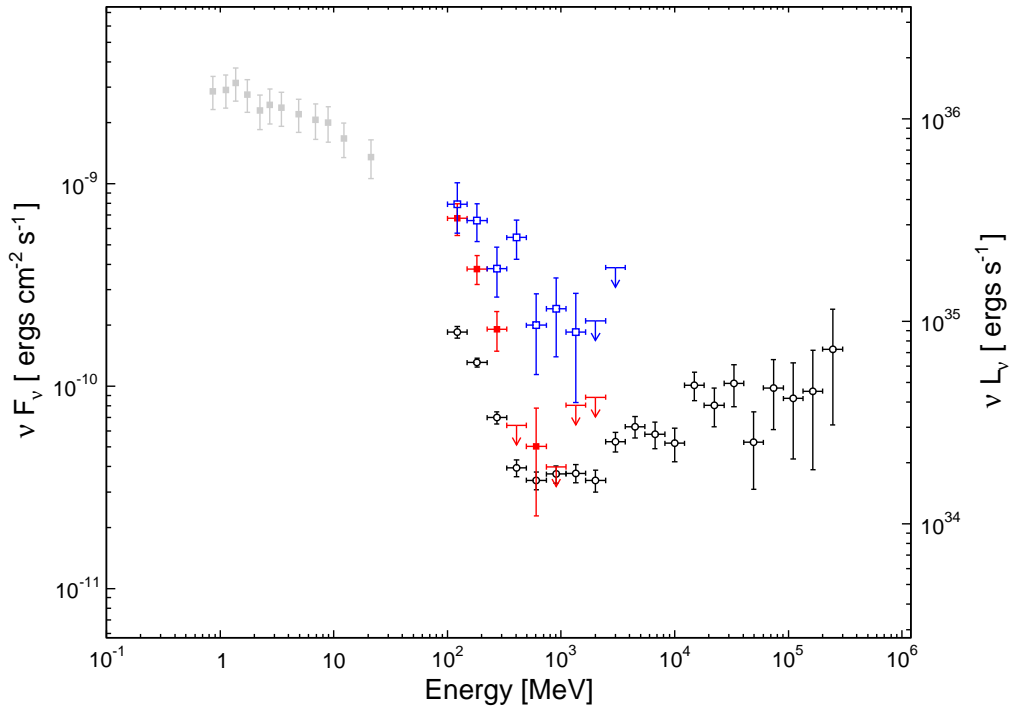


Figure 1: Spectral energy distribution of the Crab Nebula. Black open circles show the average spectrum measured by the LAT in the first 25 months of observations. Red boxes show the energy spectrum during the flare of February 2009 (MJD 54857.73-54873.73) and blue open boxes the spectrum in September 2010 (MJD 55457.73-55461.73). Gray boxes show historical data from the COMPTEL telescope (39). Arrows indicate 95% confidence flux limits.

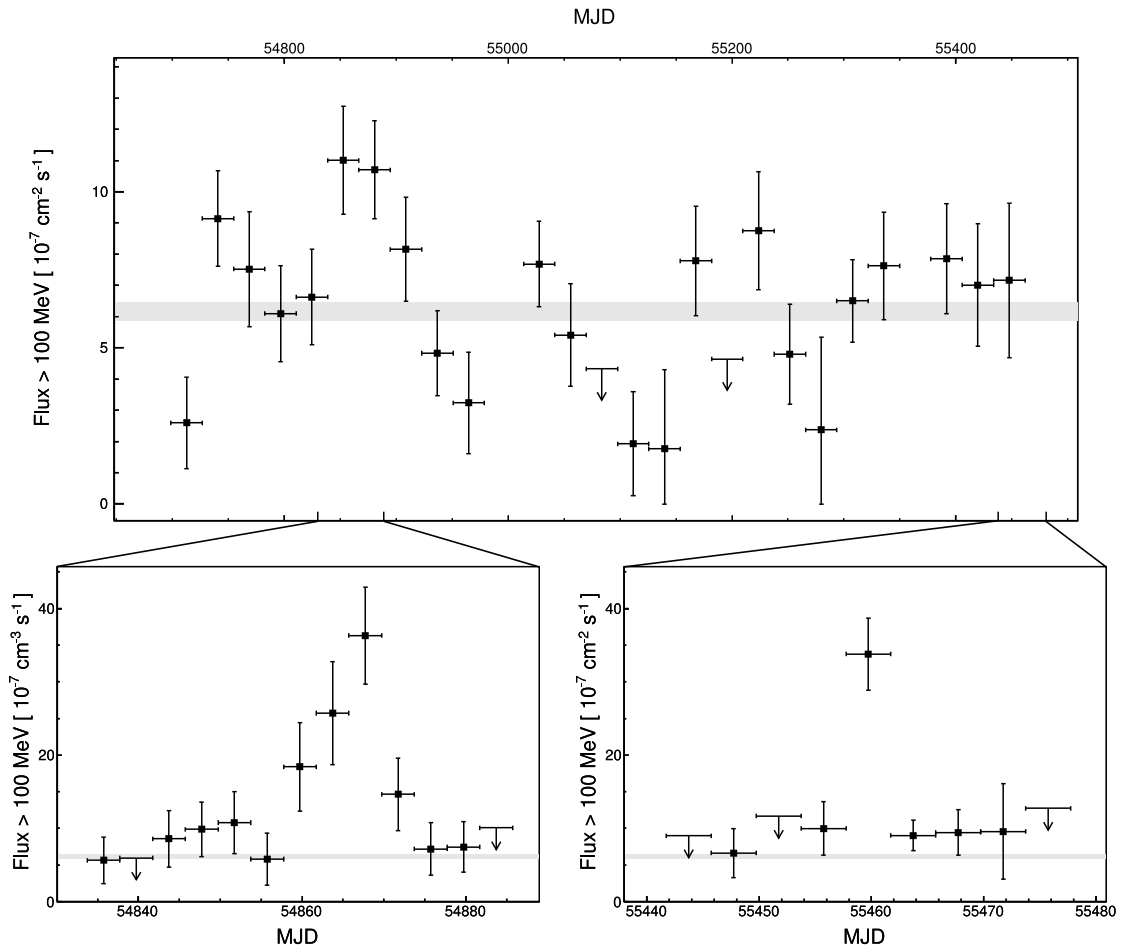


Figure 2: Gamma-ray flux above 100 MeV as a function of time of the synchrotron component of the Crab Nebula. The upper panel shows the flux in four-week intervals for the first 25 month of observations. Data for times when the sun was within 15° of the Crab Nebula have been omitted. The gray band indicates the average flux measured over the entire period. The lower panel shows the flux as a function of time in four-day time bins during the flaring periods in February 2009 and September 2010. Arrows indicate 95% confidence flux limits.

Supplements

Fermi-LAT Analysis

The LAT analysis presented in this publication was performed using the Science Tools v9r17p0 with the P6_V3_DIFFUSE instrument response functions (40). Fluxes were estimated by maximizing the likelihood of a given source model using the unbinned glike tool. The model was composed of the Galactic and isotropic diffuse models (v02 (41)), as well as all sources within 15° of the Crab pulsar in the first Fermi LAT catalog (1FGL (41)). Only photons within this same radius and with energies greater than 100 MeV were considered. All data taken under optimal conditions between MJD 54684.73 and 55477.73 were considered, except for periods when the sun was within 15° of the Crab Nebula. To avoid background contamination from the gamma-ray emission of the earth limb only time periods where the Crab Nebula was at a zenith angle $<90^\circ$ were considered. In order to avoid the strong foreground emission of the pulsar, only rotational phases between 0.52 and 0.87 were considered for the nebula analysis (22). The pulsar timing model used will be made available through the Fermi Science Support Center (40).

Light curves were generated by performing the likelihood fit in each time bin independently. The free parameters in the 28-day likelihood fits were the fluxes and spectral indices of the synchrotron and IC components of the nebula and the amplitude of the Galactic and isotropic diffuse emission. All other parameters were held fixed to their 1FGL values. In the 4-day light curves, the only free parameters of the likelihood fits were the flux and spectral index of the synchrotron component. The IC flux and spectral index and the Galactic and isotropic diffuse normalizations were held fixed to their 25-month best-fit values. Spectral data points on the SED were measured by performing the likelihood fit in each energy bin independently, varying only the normalization of the best-fit model. For both light curves and energy spectra, 95% confidence upper limits on the flux were derived if the significance of the source detection was below 2σ .

Significance and position of the flares

The flaring periods were identified by fitting a flaring component together with the average 25-month spectral model in weekly time bins between MJD 54684.73 and 55461.73. The average model included the two components of the Crab Nebula. The flaring component was modeled by a power-law energy spectrum and its normalization and index were the only parameters varied in the fits. The significance of the flaring component was $<3.5\sigma$ for all weeks outside of the flare periods, while it was $>6.7\sigma$ during the flares. Considering trials for the 102 analyzed weeks this corresponds to significances <2 and $>6\sigma$ respectively. To measure the properties of the emission during the flare in more detail two flaring periods were defined from the 4 day light curves shown in Figure 2. For the first flare the flaring period was defined as MJD 54857.73-54873.73 (the four high flux bins around the flare). Fitting the additional source with the average best-fit model yields a significance of $>8\sigma$ for the flaring component. For the

second flare the flaring period was defined as MJD 55457.73-55461.73. The significance of the flaring component during this time period is $>10 \sigma$.

For both flares the position of the flaring component was derived using the `gtfindsrc` program of the Science Tools. Both positions are compatible with the Crab Nebula. The best-fit position of the first flare is R.A.: 83.73° , Dec: 21.81° with a 68% containment radius of 0.22° (J2000), one standard deviation away from the Crab pulsar position of R.A.: 83.63° Dec: 22.01° . The best-fit position of the second flare is R.A.: 83.68° , Dec: 22.03° with a 68% containment radius of 0.044° , 1.1σ away from the pulsar.

The possibility of a background blazar

The monthly flux variability and flaring periods in principle might be due to the emission of a background source that cannot be resolved within the angular resolution of the LAT. However, this scenario is very unlikely for several reasons. First, the flux increase during both flares above 100 MeV was $\gtrsim 2 \times 10^{-6} \text{ cm}^{-2}$; there are fewer than 100 LAT sources which show variability of this magnitude. The probability of chance coincidence for one of them to be located behind the Crab Nebula within the 2σ localization error measured for the second flare, is $<6 \times 10^{-5}$. Second, the spectral index during the first flare is the softest of any source yet detected by the LAT, with the exception of the synchrotron component of the Crab Nebula itself (22, 41), suggesting that the emission originate from the same source (this argument also relates the second flare to the Crab Nebula, as the probability that both flares are produced by two different sources is negligible, due to the even lower chance probability of positional coincidence in this case). Finally, the only source class known to produce variability on the flare time scales of the observed magnitude in gamma-rays are blazars. No known blazar is located near the Crab Nebula within the angular resolution of Fermi and X-ray observations taken two days after the second flare revealed no new source which might be associated with a yet-unknown blazar (42).

Systematic Uncertainties

Stability of flux measurements with the LAT data over time was tested using sources which are expected to be constant in flux. These sources are the Crab pulsar, the nearby Geminga pulsar, the Vela pulsar and the Galactic diffuse emission. We found the light curve of each of these reference sources was consistent with a constant on monthly and 4-day timescales if we added a 5% systematic error in quadrature with the statistical errors. We have therefore added a 5% systematic error in quadrature to all light curves in this publication and have taken this systematic error to be time-variable and normally distributed. We adopt 30% as the systematic uncertainty for overall normalization of integrated fluxes $>100 \text{ MeV}$ reported here. The errors given on LAT spectral points are statistical only. The uncertainties in the energy dependence of the acceptance of the LAT leads to a systematic error of 0.1 on the photon index (22).

References and Notes

1. V. Trimble, *Publications of the Astronomical Society of the Pacific* **85**, 579 (1973).
2. M. J. Rees, J. E. Gunn, *Monthly Notices of the Royal Astronomical Society* **167**, 1 (1974).
3. C. F. Kennel, F. V. Coroniti, *The Astrophysical Journal* **283**, 710 (1984).
4. J. J. Hester, *Annual Review of Astronomy and Astrophysics* **46**, 127 (2008).
5. B. M. Gaensler, P. O. Slane, *Annual Review of Astronomy and Astrophysics* **44**, 17 (2006).
6. M. C. Weisskopf, *et al.*, *The Astrophysical Journal* **536**, L81 (2000).
7. J. D. Scargle, *The Astrophysical Journal* **156**, 401 (1969).
8. J. J. Hester, *et al.*, *The Astrophysical Journal* **577**, L49 (2002).
9. W. J. Cocke, M. J. Disney, G. W. Muncaster, *Nature* **227**, 1327 (1970).
10. R. Novick, M. C. Weisskopf, R. Berthelsdorf, R. Linke, R. S. Wolff, *The Astrophysical Journal* **174**, L1 (1972).
11. A. J. Dean, *et al.*, *Science* **321**, 1183 (2008).
12. R. J. Gould, G. R. Burbidge, *Annales d'Astrophysique* **28**, 171 (1965).
13. A. M. Atoyan, F. A. Aharonian, *Monthly Notices of the Royal Astronomical Society* **278**, 525 (1996).
14. M. C. Weisskopf, *et al.*, *The Astrophysical Journal* **713**, 912 (2010).
15. M. Meyer, D. Horns, H. S. Zechlin, The crab nebula as a standard candle in very high-energy astrophysics, <http://adsabs.harvard.edu/abs/2010arXiv1008.4524M> (2010).
16. C. A. Wilson-Hodge, *et al.*, When a standard candle flickers, <http://adsabs.harvard.edu/abs/2010arXiv1010.2679W> (2010).
17. R. Much, *et al.*, *Astronomy and Astrophysics* **299**, 435 (1995).
18. O. C. de Jager, *et al.*, *The Astrophysical Journal* **457**, 253 (1996).
19. F. Aharonian, *et al.*, *The Astrophysical Journal* **614**, 897 (2004).
20. F. Aharonian, *et al.*, *Astronomy and Astrophysics* **457**, 899 (2006).
21. J. Albert, *et al.*, *The Astrophysical Journal* **674**, 1037 (2008).

22. A. A. Abdo, *et al.*, *The Astrophysical Journal* **708**, 1254 (2010).
23. M. Tavani, *et al.*, Agile detection of enhanced gamma-ray emission from the crab nebula region, Astronomers telegramm 2855, <http://www.astronomerstelegam.org> (2010).
24. Astronomers telegramms: 2867, 2872, 2893, <http://www.astronomerstelegam.org> (2010).
25. M. Ajello, *et al.*, *The Astrophysical Journal* **673**, 96 (2008).
26. Bat digest, http://heasarc.gsfc.nasa.gov/docs/swift/analysis/bat_digest.html.
27. Astronomical telegramms: 2882,2903, <http://www.astronomerstelegam.org> (2010).
28. S. S. Komissarov, Y. E. Lyubarsky, *Monthly Notices of the Royal Astronomical Society* **349**, 779 (2004).
29. L. D. Zanna, D. Volpi, E. Amato, N. Bucciantini, *Astronomy and Astrophysics* **453**, 621 (2006).
30. N. F. Camus, S. S. Komissarov, N. Bucciantini, P. A. Hughes, *Monthly Notices of the Royal Astronomical Society* **400**, 1241 (2009).
31. A. M. Atoyan, F. A. Aharonian, *Astronomy and Astrophysics Supplement Series* **120**, 453 (1996).
32. J. J. Hester, *et al.*, *The Astrophysical Journal* **448**, 240 (1995).
33. O. C. de Jager, A. K. Harding, *The Astrophysical Journal* **396**, 161 (1992).
34. M. Lyutikov, *MNRAS* **405**, 1809 (2010).
35. Y. A. Gallant (2002), vol. 589, p. 24.
36. E. Amato, J. Arons, *The Astrophysical Journal* **653**, 325 (2006).
37. N. Bucciantini, J. Arons, E. Amato, *MNRAS* pp. 1423–+ (2010).
38. R. D. Blandford, *Lighthouses of the Universe: The Most Luminous Celestial Objects and Their Use for Cosmology*, M. Gilfanov, R. Sunyeav, & E. Churazov, ed. (2002), pp. 381–+.
39. L. Kuiper, *et al.*, *Astronomy and Astrophysics* **378**, 918 (2001).
40. Fermi science support center, <http://fermi.gsfc.nasa.gov/ssc/data/analysis/scitools/overview.html>.
41. A. A. Abdo, *et al.*, *The Astrophysical Journal Supplement Series* **188**, 405 (2010).
42. C. O. Heinke, Swift imaging shows no evidence for active agn near crab, Astronomers telegramm 2872, <http://www.astronomerstelegam.org> (2010).